Chinese Chemical Letters 34 (2023) 108126

Contents lists available at ScienceDirect

Chinese Chemical Letters

journal homepage: www.elsevier.com/locate/cclet

Effect of spatial configuration on adhesion of 1,2-disubstituted cyclohexane derivatives

Qiao Zhang[a], Yuhang Yin[b], Jingfu Song[b], Gai Zhao[b,*], Shengyi Dong[a,*]

[a] College of Chemistry and Chemical Engineering, Hunan University, Changsha 410082, China
[b] State Key Laboratory of Mechanics and Control of Mechanical Structures, Nanjing University of Aeronautics and Astronautics, Nanjing 210016, China

ARTICLE INFO

Article history:
Received 6 October 2022
Revised 25 December 2022
Accepted 27 December 2022
Available online 30 December 2022

Keywords:
Spatial configuration
Supramolecular adhesive material
Assembly
Cohesion
Adhesion

ABSTRACT

Spatial configuration has a significant effect on chemical self-assembly. However, the importance of spatial configuration in supramolecular adhesive materials has been frequently ignored. In this study, the effects of the spatial configuration on cohesion and adhesion were investigated. Owing to the diversities of the chemical structures and assembly patterns, 1,2-disubstituted cyclohexane derivatives were used in this combined experimental and theoretical investigation. The self-sorting assembly of enantiopure isomers improved cohesion but had a negative effect on adhesion. In contrast, racemic mixtures displayed stronger adhesion effects. Moreover, it was proven that the *cis*-configuration was more favorable for supramolecular adhesion than the *trans*-counterpart. In addition, the influence of the spatial configuration of 1,2-disubstituted cyclohexane derivatives could be effectively mitigated by hydrogen bond donors or acceptors. The addition of natural acids yielded three-dimensional polymeric networks, in which the spatial configuration was not the decisive factor for supramolecular adhesion.

Self-assembly has been established as a powerful medium for providing spatial configuration beyond the molecular level [1–4]. The transformation or amplification of chirality from building blocks to chemical assemblies provides supramolecular materials with structural and functional specificities [5–8]. In nature, supramolecular adhesion is widely prevalent in biological activities [9–12]. Non-covalent interaction and spatial configuration can be considered as two sides of a coin in adhesion, and play active roles in adhesion effects [13–15]. On the one hand, adhesive units apply non-covalent forces to realize remarkable affinities to surfaces; on the other hand, spatial configuration affects the self-assembly pattern and interaction mode of adhesive structures [16–18]. Therefore, understanding the importance of the non-covalent interaction and spatial configuration in supramolecular adhesion is essential. Over the past decade, many studies have attempted to investigate the key role played by adhesion interactions [19–22]. However, spatial information on adhesive materials with chiral components has been neglected in practical adhesion studies [23–25].

The analysis of 1,2-disubstituted cyclohexane offers abundant information on the spatial configuration of diverse stereoisomers [26–28]. The variability of enantiomers/diastereoisomers render them highly promising for investigating the importance of the spatial configuration in supramolecular adhesion [29–31]. Amorphous structures usually exhibit stronger adhesion effects than structurally ordered or crystallized structures [32–34]. Hence, the spatial configuration of 1,2-disubstituted cyclohexane derivatives must be studied in the amorphous bulk state, which has been challenging thus far.

One feasible strategy to study the spatial configuration in bulk materials is to combine theoretical analysis with experimental investigation [35,36]. In this study, such a combined approach was adopted to study the spatial configuration provided by supramolecular adhesion. *trans*/*cis*-1,2-Disubstituted cyclohexanes were selected as chiral sources to express the diversity of the spatial configuration. Benzo-21-crown-7 (B21C7) is a macrocyclic ether containing multiple oxygen, which can form multiple hydrogen bond interactions and is widely used in the preparation of supramolecular adhesive materials [37,38]. B21C7 units were connected to cyclohexane rings as functional units for supramolecular adhesion. With the assistance of chiral 1,2-disubstituted cyclohexane cores, the spatial configuration was found to have a considerable effect on supramolecular adhesion.

In this study, three *trans*/*cis*-1,2-disubstituted cyclohexane derivatives with B21C7 units were designed and synthesized (Fig. 1a). All monomers were purified using silica gel chromatography and fully characterized. Detailed information on the prepa-

* Corresponding authors.
E-mail addresses: zhaogai@nuaa.edu.cn (G. Zhao), dongsy@hnu.edu.cn (S. Dong).

https://doi.org/10.1016/j.cclet.2022.108126
1001-8417/

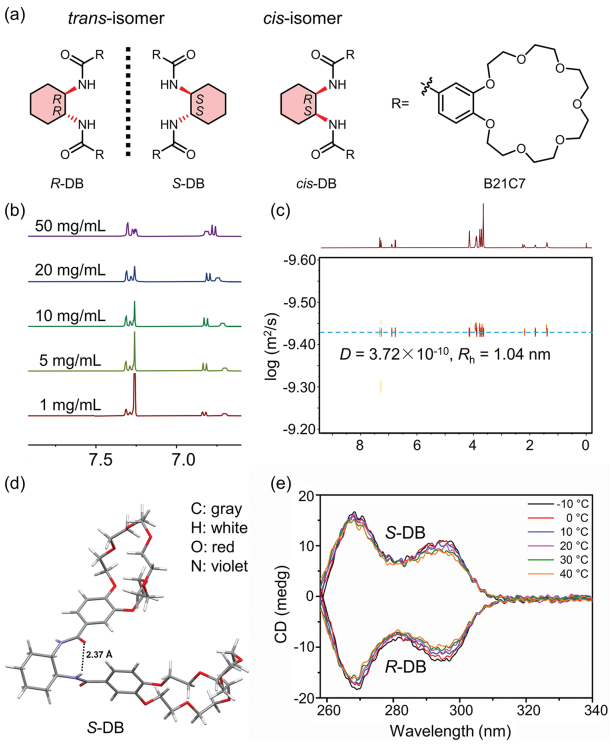

Fig. 1. (a) Structures of *R*-DB, *S*-DB, *cis*-DB; (b) Concentration-dependent ^{1}H NMR of *S*-DB in $CDCl_3$; (c) DOSY spectra of *S*-DB in $CDCl_3$ (50 mg/mL); (d) The optimized geometry of *S*-DB (at the B3LYP/6–311G(d) level of theory); (e) Temperature-dependent CD spectra of *S*-DB and *R*-DB in $CHCl_3$ (0.02 mg/mL).

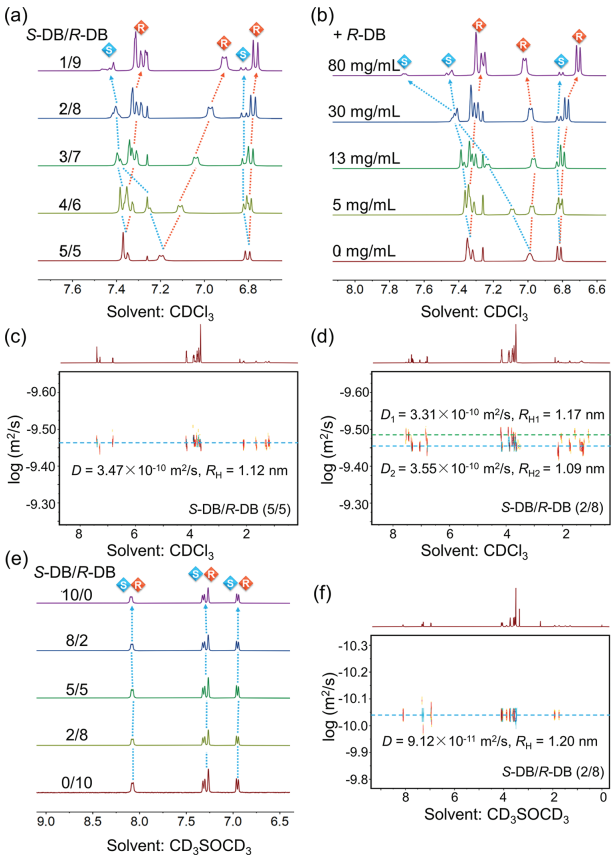

Fig. 2. Self-assembly of the mixtures of *S*-DB and *R*-DB in solution. (a) ^{1}H NMR spectra of the mixture of *S*-DB and *R*-DB in $CDCl_3$ (50 mg/mL); (b) ^{1}H NMR titration spectra of *rac*-DB (20 mg/mL) with *R*-DB in $CDCl_3$; (c) DOSY spectra of *rac*-DB in $CDCl_3$ (50 mg/mL); (d) DOSY spectra of $[S\text{-DB/R-DB}]_{2/8}$ in $CDCl_3$ (50 mg/mL); (e) ^{1}H NMR spectra of the mixture of *S*-DB and *R*-DB in CD_3SOCD_3 (50 mg/mL); (f) DOSY spectra of $[S\text{-DB/R-DB}]_{2/8}$ in CD_3SOCD_3 (50 mg/mL).

ration and characterization is provided in Supporting information (Figs. S1–S8 in Supporting information). In particular, the purities of the monomers were checked using high performance liquid chromatography (HPLC) and chiral HPLC (Figs. S9–S13 in Supporting information). Before investigating the spatial configuration of *S*-DB, *R*-DB and *cis*-DB in the solid state, their organization patterns, including stereoisomerism, were studied in solution.

No supramolecular polymerization of *S*-DB was observed in concentration-dependent ^{1}H NMR tests (Fig. 1b and Figs. S14–S19 in Supporting information). For example, when the concentration of *S*-DB was increased to 50 mg/mL, the peak shapes of the protons from *S*-DB were still clearly recorded, indicating the absence of polymeric structures (Fig. 1b and Fig. S14) [39]. More detailed information was provided by diffusion-ordered spectroscopy (DOSY) experiments (Fig. 1c and Figs. S20–S22 in Supporting information). The diffusion coefficient of *S*-DB at 50 mg/mL is 3.72×10^{-10} m^2/s (1.04 nm), demonstrating that *S*-DB existed in the monomeric state in the concentrated solution (Fig. 1c). In H/D exchange experiments, the –CONH– units in the chiral core could not be transferred to –COND–, indicating the existence of intramolecular hydrogen bonds in the amide groups (Figs. S23–S25 in Supporting information) [37]. Analysis of the chemical structures of *S*-DB and *R*-DB showed that the existence of B21C7 units resulted in the water molecules favouring the formation of hydrogen bonds with B21C7 rather than with the amide groups (no H/D exchange) [37]. The distance between the two amide groups in the optimized structure of *S*-DB is 2.37 Å, supporting the occurrence of intramolecular hydrogen bonding (Fig. 1d and Fig. S26 in Supporting information) [40]. The replacement of *S*-DB with *R*-DB or *cis*-DB resulted in the same observations (Figs. S15–S26). No distinct changes were observed in the temperature-dependent circular dichroism (CD) measurements of *S*-DB or *R*-DB, indicating that the chirality of either of them exclusively originated from the 1,2-disubstituted cyclohexane core (Fig. 1e) [28]. No CD signal was observed in the spectrum of *cis*-DB, suggesting its mesomeric feature (Fig. S31 in Supporting information).

Based on the aforementioned information, investigations were focused on the assembly pattern of mixtures of *S*-DB and *R*-DB (Fig. 2 and Figs. S36–S54 in Supporting information). In the ^{1}H NMR spectrum of *S*-DB/*R*-DB (5:5, 50 mg/mL, $CDCl_3$), only one set of proton peaks was observed (Fig. 2a and Fig. S36). However, when the mole ratios of *S*-DB/*R*-DB were not identical, peaks assigned to *S*-DB or *R*-DB were easily and clearly identified, respectively (Fig. 2a and Fig. S36). Fig. 2b and Fig. S37 show the typical self-sorting behavior of *S*-DB and *R*-DB in $CDCl_3$ [41]. The addition of *R*-DB to *rac*-DB resulted in peaks of *R*-DB and *S*-DB that were distinct from those of *rac*-DB. Decisive evidences was obtained from DOSY experiments (Figs. 2c and d, Figs. S44–S48). A single set of proton peaks was observed in the DOSY spectra of *S*-DB/*R*-DB (5:5, 50 mg/mL, $CDCl_3$) (Fig. 2c). However, two sets of proton peaks were observed in the DOSY spectra of *S*-DB/*R*-DB (2:8, 50 mg/mL, $CDCl_3$), indicating its self-sorting behavior in the solution state (Fig. 2d) [42]. An inverse *S*-DB/*R*-DB molar ratio of 8:2 led to the same self-sorting result (Fig. S46). Calculation of the average molecular sizes of *S*-DB (1.17 nm) and *R*-DB (1.09 nm) in the *S*-DB/*R*-DB mixtures showed that *S*-DB and *R*-DB were in the monomeric state.

The self-sorting pattern of *S*-DB and *R*-DB only occurred in $CDCl_3$. A small amount of CD_3SOCD_3 molecules alleviated the self-sorting behavior of the *S*-DB/*R*-DB mixtures (Figs. 2e and f, Figs. S38 and S39). No self-sorting behavior of *S*-DB/*R*-DB (2:8) was observed in CD_3SOCD_3 (Fig. 2e and Fig. S39). One set of diffu-

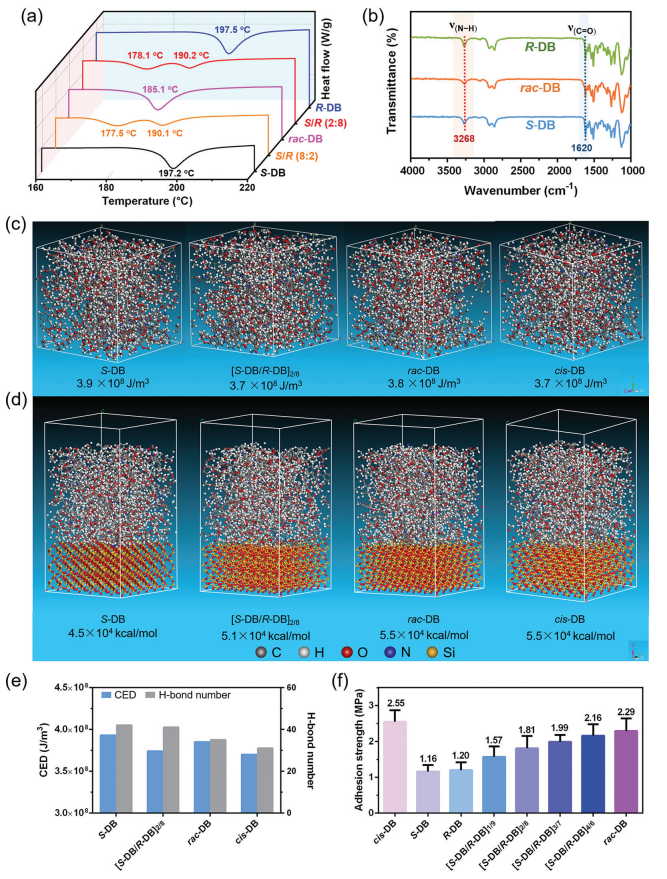

Fig. 3. Self-assembly of *S*-DB, *R*-DB and *rac*-DB in solid: (a) DSC measurements of *S*-DB, *R*-DB and *S*-DB/*R*-DB mixtures; (b) IR spectra of *S*-DB, *R*-DB and *rac*-DB. Adhesion and cohesion of *trans*/*cis*-DB: (c) The cohesive energy density (CED) of *trans*/*cis*-DB ($3.3 \times 3.3 \times 3.3\,nm^3$); (d) The interaction potential energy ($E_{interfacial}$) between *trans*/*cis*-DB ($3.3 \times 3.3 \times 4.4\,nm^3$) and glass ($3.3 \times 3.3 \times 1.6\,nm^3$) at 298.15 K; (e) Summary of CED and H-bond number of *trans*/*cis*-DB; (f) Adhesion strengths of *trans*/*cis*-DB to glass.

sion coefficients was obtained in the DOSY experiment (*S*-DB/*R*-DB, 2:8, 50 mg/mL, CD_3SOCD_3), indicating that intramolecular hydrogen bonding was disrupted by CD_3SOCD_3 (Fig. 2f) [43]. Thus, the self-sorting assembly pattern in *S*-DB/*R*-DB mixtures was induced by intramolecular hydrogen bonding. In contrast, it was easy to distinguish the NMR peaks of *S*-DB and *R*-DB from the NMR spectra of the *S*-DB/*cis*-DB mixtures and *R*-DB/*cis*-DB mixtures, respectively (Figs. S40–S43). Two sets of diffusion coefficients were observed in the DOSY spectra of *R*-DB/*cis*-DB ($CDCl_3$ or CD_3SOCD_3, Figs. S47 and S48). *R*-DB, *S*-DB and *cis*-DB were found in the monomeric states. These results indicate that *trans*- and *cis*-monomers have different spatial configurations, an observation that will be helpful for understanding the adhesion performances of *S*-DB, *R*-DB and *cis*-DB.

Pure *S*-DB and *R*-DB are white solids, whereas *cis*-DB is a gel-like material that becomes a white solid after prolonged storage (100 days) at 25 °C. This demonstrates the importance of spatial configuration in the material properties. Compared to the amorphous nature of *cis*-DB, the spatial configurations of the *trans*-structures can increase the crystallinity of *S*-DB and *R*-DB (Fig. S61). However, the racemic mixture of *S*-DB and *R*-DB showed reduced crystallization, which is favorable for supramolecular adhesion (Fig. S61) [37,38]. Differential scanning calorimeter (DCS) measurements revealed the assembly patterns of *S*-DB and *R*-DB in the solid state (Fig. 3a and Fig. S63). As shown in Fig. 3a, *trans*-isomers (*S*-DB and *R*-DB) exhibited a melting point (T_m) at approximately 197 °C (197.2 and 197.5 °C), whereas *rac*-DB (*S*-DB/*R*-DB, 1:1) showed T_m at 185.2 °C, which is a typical feature of conglomerates [44,45]. The lower T_m of *rac*-DB may originate from the weak interactions between the B21C7 units [37,38]. In contrast, the simply mixed *S*-DB/*R*-DB (1:1) has a T_m of 192.4 °C (Fig. S63). Meanwhile, *S*-DB/*R*-DB with non-equivalent molar ratios showed two distinct melting points in the DSC curves, indicating a self-sorting organization pattern in the *S*-DB/*R*-DB mixtures (Fig. 3a and Fig. S63). The IR spectra of *S*-DB and *R*-DB showed bands at 3268 and 1620 cm^{-1}, corresponding to hydrogen-bonded $s_{(N-H)}$ and $d_{(C=O)}$, respectively. However, *rac*-DB showed peaks at the similar wavenumbers as those of *S*-DB and *R*-DB (Fig. 3b and Fig. S64 in Supporting information). Thus, the interaction of *S*-DB/*S*-DB (or *R*-DB/*R*-DB) is stronger than that of *S*-DB/*R*-DB in the solid state [28,46]. Simulation results provided more detailed information. The combination energy of *S*-DB/*S*-DB is −40.8 kcal/mol, while that of *S*-DB/*R*-DB is −25.9 kcal/mol, indicating that *S*-DB tends to bind with *S*-DB rather than with *R*-DB (Fig. S65 in Supporting information).

Before the macroscopic supramolecular adhesion tests, the relationships among the spatial configuration, cohesion effect, and adhesion effect were investigated (Figs. 3c–f and Figs. S66–S68 in Supporting information). As shown in Fig. 3c, the cohesion energy density of *S*-DB is $3.9 \times 10^8\,J/m^3$. The cohesion energies of the *S*-DB/*R*-DB mixtures are slightly lower than that of *S*-DB, with that of *S*-DB/*R*-DB (2:8) equal to $3.7 \times 10^8\,J/m^3$. The *cis*-spatial configuration (*cis*-DB) has a relatively lower cohesion energy ($3.7 \times 10^8\,J/m^3$) than the *trans*-counterparts. In aggregated clusters with the same number of molecules ($3.3 \times 3.3 \times 3.3\,nm^3$), *S*-DB has more hydrogen bonds (42) than that of the *S*-DB/*R*-DB mixture (5:5, 35) (Fig. 3e and Table S2 in Supporting information), indicating that the mixing of *S*-DB and *R*-DB effectively attenuates the intermolecular interactions. In addition, *cis*-DB has less hydrogen bonds (31) than the *trans*-counterparts (Fig. 3f and Table S2). However, the adhesion behavior is controlled by cohesion and adhesion effects, with the weaker effect being the decisive factor [47,48]. Considering that *S*-DB, *R*-DB, *S*-DB/*R*-DB mixtures and *cis*-DB have similar cohesion effects, the adhesion effects are more important. Subsequently, the adhesion mode were simulated by calculating interaction energy between DB and glass. Different from the results obtained by the cohesion energy density, *S*-DB and *R*-DB showed weak adhesion energies to glass. In contrast, *cis*-DB and *rac*-DB have higher adhesion energies (Fig. 3d). Macroscopic adhesion tests confirmed the simulation results. Adhesion failure of *S*-DB or *R*-DB was observed in the weight loading tests, whereas cohesion failure was observed when *cis*-DB or *S*-DB/*R*-DB (5/5) was used (Fig. S68).

Macroscopic lap-shear measurements of *S*-DB, *R*-DB, *cis*-DB, and *S*-DB/*R*-DB mixtures were performed to quantitatively evaluate their adhesive abilities (Fig. 3f). Enantiopure *S*-DB and *R*-DB showed adhesion strengths of 1.16 and 1.20 MPa, respectively, to glass. Adding *S*-DB to *R*-DB can effectively enhance the adhesion effects. The mixtures of *S*-DB/*R*-DB with molar ratios of 1:9 and 3:7 show adhesion strengths of 1.57 and 1.99 MPa, respectively. The strongest adhesion performance of the *S*-DB/*R*-DB series was achieved by a racemic mixture of *S*-DB and *R*-DB (5:5), with an adhesion strength of 2.29 MPa. Meanwhile, *cis*-DB exhibited an adhesion strength of 2.55 MPa, which is approximately 1.1 to 2.2 times higher than that of the *S*-DB/*R*-DB series. In our previous studies, we demonstrated that amorphous structures are helpful for supramolecular adhesion [49]. *S*-DB or *R*-DB favors the formation of ordered structures in the solid state, which mitigates the interactions with the adhered surfaces (adhesion effect). The addition of *R*-DB to *S*-DB (or *S*-DB to *R*-DB) can partially weaken the ordered self-assembly pattern, resulting in a stronger adhesion effect.

To further study the spatial configuration in supramolecular adhesion, natural acids with hydrogen bonding sites were introduced

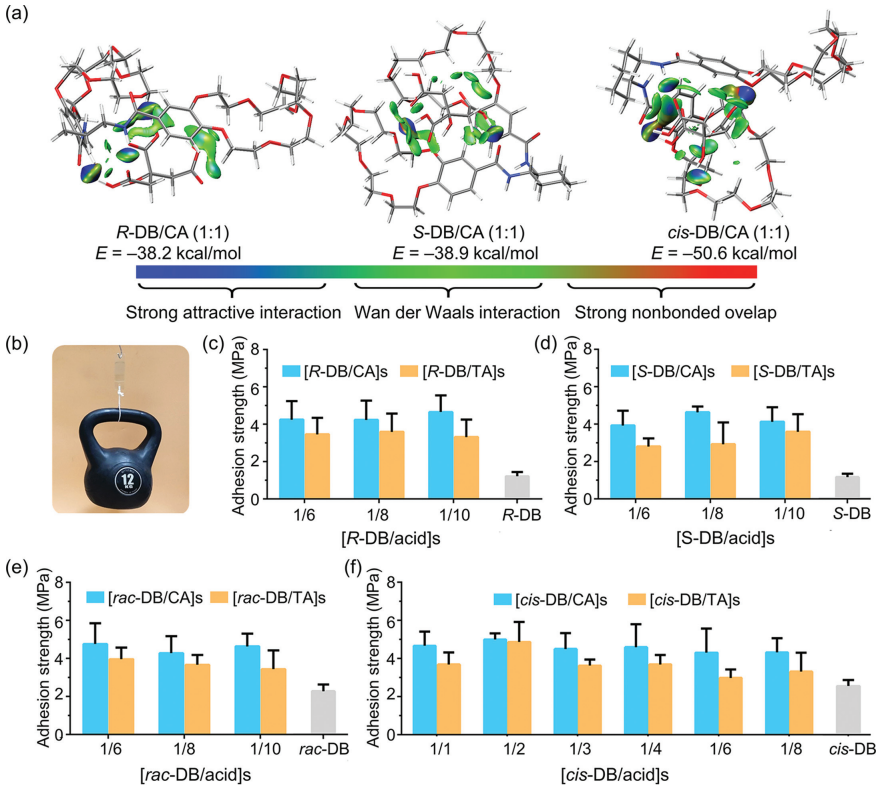

Fig. 4. Adhesion behavior of DB and natural acids. (a) The combination energy (*E*) of *R*-DB/CA (molar ratio 1:1), *S*-DB/CA (molar ratio 1:1) and *cis*-DB/CA (molar ratio 1:1); (b) Macroscopic tests of adhesion behavior of $[cis\text{-DB/CA}]_{1/2}$ (adhesion areas are $3.0 \times 6.0\,cm^2$); (c) Adhesion strengths of [*R*-DB/CA]s and [*R*-DB/TA]s to glass; (d) Adhesion strengths of [*S*-DB/CA]s and [*S*-DB/TA]s to glass; (e) Adhesion strengths of [*rac*-DB/CA]s and [*rac*-DB/TA]s to glass; (f) Adhesion strengths of [*cis*-DB/CA]s and [*cis*-DB/TA]s to glass. These adhesion results clearly indicate the importance of the spatial configuration in supramolecular adhesion. First, the *cis*-spatial configuration is more favorable for supramolecular adhesion than the *trans*-spatial configuration. Second, the spatial configurations of *trans*/*cis*-1,2-disubstituted cyclohexane derivatives have a greater influence on adhesion than on cohesion. Third, racemic mixtures of *S*-DB/*R*-DB exhibit stronger adhesion than *S*-DB or *R*-DB.

into the 1,2-disubstituted cyclohexane systems (Fig. 4 and Fig. S69 in Supporting information). Citric acid (CA) and DL-tartaric acid (TA) were used as exotic components to form hydrogen bonds with the 1,2-disubstituted cyclohexane derivatives. The addition of CA or TA drastically changed the morphology of these derivatives (Fig. S69). Freshly prepared acid-cyclohexane materials were highly viscous liquids, as confirmed by macroscopic tests and rheological experiments Fig. 4b, Figs. S71 and S72 in Supporting information). No covalent bonding between the acids and 1,2-disubstituted cyclohexane derivatives was observed, indicating non-covalent interactions between them (Figs. S74-S81 in Supporting information). Meanwhile, the acid-cyclohexane materials were amorphous without any sign of crystallization (Fig. S91 in Supporting information). Combining these results and the results obtained from our previous work, we demonstrated that natural acids form deep eutectic supramolecular polymers with 1,2-disubstituted cyclohexane derivatives [50]. In polymeric structures, natural acids connect with 1,2-disubstituted cyclohexane derivatives *via* hydrogen bonds to form three-dimensional networks [51]. They are highly cross-linked in the polymeric networks and no self-sorting organization occurs. Simulation calculation results showed the hydrogen bonding between CA and amide groups of 1,2-disubstituted cyclohexanes, indicating that chiral information is profoundly affected by the addition of natural acids.

The combination energies of *R*-DB/CA and *S*-DB/CA are −38.2 kcal/mol and −38.9 kcal/mol, indicating strong binding capacity with CA (Fig. 4a). *cis*-DB exhibited stronger binding properties with CA (−50.6 kcal/mol) (Fig. 4a). These simulation results are consistent with the results obtained from the macroscopic adhesion tests, in that the incorporation of TA or CA significantly increased the adhesion strength of 1,2-disubstituted cyclohexane derivatives (Figs. 4c–f and Figs. S98–S101 in Supporting information). For example, the [*R*-DB/CA] and [*R*-DB/TA] series showed adhesion strengths up to 4.66 and 3.60 MPa, respectively (Fig. 4c). These are much higher than that of *R*-DB (1.20 MPa). Similarly, enhanced adhesion effects were observed when *R*-DB was replaced with *S*-DB (Fig. 4d). The addition of acids to racemic mixtures also increased the adhesion performance. Two adhesion strengths of 4.76 and 3.96 MPa were recorded for the [*rac*-DB/CA] and [*rac*-DB/TA] series, respectively (Fig. 4e). Comparison of the adhesion strengths of acid/*R*-DB, acid/*S*-DB, and acid/*rac*-DB revealed that they were similar, and that the adhesion effects of acid/*rac*-DB were not considerably stronger. A reasonable explanation is that the spatial configuration-induced adhesion differences were fully mitigated owing to supramolecular polymerization. Adhesion observations obtained from acid/*cis*-DB confirmed this explanation. The highest adhesion strengths of the [*cis*-DB/CA] and [*cis*-DB/TA] series were 5.00 and 4.87 MPa (Fig. 4f), respectively, to glass, which are slightly higher than those of the [*rac*-DB/CA] (4.76 MPa) and [*rac*-DB/TA] series (3.96 MPa). It is clear that the addition of natural acids significantly diminished the adhesion differences induced by the spatial configuration.

In conclusion, the importance of the spatial configuration in supramolecular adhesion was studied. 1,2-Disubstituted cyclohexane derivatives with B21C7 units were used in the experimental and theoretical investigations. The *cis*- and *trans*-structures have different influences on the adhesion performances, with the former showing stronger adhesion effects. The racemic mixtures exhibited stronger adhesion effects than the enantiomers. The adhesion differences caused by the *trans*/*cis*-spatial configuration could

be effectively mitigated by hydrogen bond formation. The addition of natural acids considerably destroyed the intrinsic assembly patterns of the 1,2-disubstituted cyclohexane derivatives and resulted in stronger adhesion performances. Thus, this study clarified the importance of the spatial configuration of adhesives in cohesion and adhesion phenomena.

Declaration of competing interest

The authors declare no conflict of interest.

Acknowledgments

The authors gratefully acknowledge the Outstanding Youth Scientist Foundation of Hunan Province (No. 2021JJ10010), the National Natural Science Foundation of China (Nos. 22271087, 21704024), the Huxiang Young Talent Program from Hunan Province (No. 2018RS3036), the Fundamental Research Funds for the Central Universities from Hunan University.

Supplementary materials

Supplementary material associated with this article can be found, in the online version, at doi:10.1016/j.cclet.2022.108126.

References

[1] S. Huang, H. Yu, Q. Li, Adv. Sci. 8 (2021) 2002132.
[2] L. Zhang, H.X. Wang, S. Li, et al., Chem. Soc. Rev. 49 (2020) 9095–9120.
[3] A. Jozeliūnaitė, T. Javorskis, V. Vaitkevičius, et al., J. Am. Chem. Soc. 144 (2022) 8231–8241.
[4] C. Liu, Z. Li, H. Yu, et al., Chin. Chem. Lett. 32 (2021) 1385–1389.
[5] P.K. Hashim, J. Bergueiro, E.W. Meijer, et al., Prog. Polym. Sci. 105 (2020) 101250.
[6] H. Zhu, Q. Li, Z. Gao, et al., Angew. Chem. Int. Ed. 59 (2020) 10868–10872.
[7] M.L. Ślęczkowski, M.F.J. Mabesoone, P. Ślęczkowski, et al., Nat. Chem. 13 (2021) 200–207.
[8] Y. Yan, X. Li, G. Chen, et al., Chin. Chem. Lett. 32 (2021) 107–112.
[9] C. Heinzmann, C. Weder, L.M. de Espinosa, Chem. Soc. Rev. 45 (2016) 342–358.
[10] Y. Zhao, Y. Wu, L. Wang, et al., Nat. Commun. 8 (2017) 2218.
[11] A.H. Hofman, I.A. van Hees, J. Yang, et al., Adv. Mater. 30 (2018) 1704640.
[12] X. Dong, H. Zhao, Z. Wang, et al., Chin. Chem. Lett. 30 (2019) 2333–2337.
[13] C. Zhang, B. Wu, Y. Zhou, et al., Chem. Soc. Rev. 49 (2020) 3605–3637.
[14] C. Cui, W. Liu, Prog. Polym. Sci. 116 (2021) 101388.
[15] S. Wu, W. Wang, C. Cai, et al., Chin. Chem. Lett. 34 (2023) 107830.
[16] Y. Chen, J. Meng, Z. Gu, et al., Adv. Funct. Mater. 20 (2020) 1905287.
[17] P. Sun, Y. Li, B. Qin, et al., ACS Mater. Lett. 3 (2021) 1003–1009.
[18] X. Huang, Z. Shangguan, Z.Y. Zhang, et al., Chem. Mater. 34 (2022) 2636–2644.
[19] X. Ji, M. Ahmed, L. Long, et al., Chem. Soc. Rev. 48 (2019) 2682–2697.
[20] M. Kim, J. Park, K.M. Lee, et al., J. Am. Chem. Soc. 144 (2022) 6261–6269.
[21] S. Chen, Z. Li, Y. Wu, et al., Angew. Chem. Int. Ed. (2022) e202203876.
[22] Y. Mao, Z. Xu, Z. He, et al., Chin. Chem. Lett. 34 (2023) 107461.
[23] L. Xie, L. Gong, J. Zhang, et al., J. Mater. Chem. A 7 (2019) 21944–21952.
[24] A. Narayanan, A. Dhinojwala, A. Joy, Chem. Soc. Rev. 50 (2021) 13321–13345.
[25] R. Bai, H. Zhang, X. Yang, et al., Polym. Chem. 13 (2022) 1253–1259.
[26] Y.L. Bennani, S. Hanessian, Chem. Rev. 97 (1997) 3161–3195.
[27] M. Li, S.H. Li, D. Zhang, et al., Angew. Chem. Int. Ed. 57 (2018) 2889–2893.
[28] C. Kulkarni, J.A. Berrocal, M. Lutz, et al., J. Am. Chem. Soc. 141 (2019) 6302–6309.
[29] X. Dou, N. Mehwish, C. Zhao, et al., Acc. Chem. Res. 53 (2020) 852–862.
[30] Y. Chen, S. Pangannaya, B. Sun, et al., ACS Appl. Bio. Mater. 4 (2021) 2066–2072.
[31] Y. Zhao, S. Song, X. Ren, et al., Chem. Rev. 122 (2022) 5604–5640.
[32] Q. Zhang, C.Y. Shi, D.H. Qu, et al., Sci. Adv. 4 (2018) eaat8192.
[33] Z. Yu, P. Wu, Mater. Horiz 8 (2021) 2057–2064.
[34] Y. Gao, J. Zhao, Z. Huang, et al., Angew. Chem. Int. Ed. (2022) e202201793.
[35] X. Li, J. Lai, Y. Deng, et al., J. Am. Chem. Soc. 142 (2020) 21522–21529.
[36] X. Li, Y. Deng, J. Lai, et al., J. Am. Chem. Soc. 142 (2020) 5371–5379.
[37] S. Dong, J. Leng, Y. Feng, et al., Sci. Adv. 3 (2017) eaao0900.
[38] Q. Zhang, T. Li, A. Duan, et al., J. Am. Chem. Soc. 141 (2019) 8058–8063.
[39] S. Wu, C. Cai, F. Li, et al., CCS Chem. 2 (2020) 1690–1700.
[40] H.J. Lee, Y.S. Choi, K.B. Lee, et al., J. Phys. Chem. A 106 (2002) 7010–7017.
[41] C. Dressel, T. Reppe, M. Prehm, et al., Nat. Chem. 6 (2014) 971–977.
[42] M.M. Safont-Sempere, G. Fernández, F. Würthner, Chem. Rev. 111 (2011) 5784–5814.
[43] K.T. Mahmudov, M.N. Kopylovich, M.F.C. Guedes da Silva, et al., Coordin. Chem. Rev. 345 (2017) 54–72.
[44] S. Dutta, A.J. Gellman, Chem. Soc. Rev. 46 (2017) 7787–7839.
[45] M. Wehner, M.I.S. Röhr, V. Stepanenko, et al., Nat. Commun. 11 (2020) 5460.
[46] J. Huang, L. Yu, J. Am. Chem. Soc. 128 (2006) 1873–1878.
[47] D. Gan, W. Xing, L. Jiang, et al., Nat. Commun. 10 (2019) 1487.
[48] S. Arias, S. Amini, J. Horsch, et al., Angew. Chem. Int. Ed. 59 (2020) 18495–18499.
[49] S. Wu, C. Cai, F. Li, et al., Angew. Chem. Int. Ed. 59 (2020) 11871–11875.
[50] B.B. Hansen, S. Spittle, B. Chen, et al., Chem. Rev. 121 (2021) 1232–1285.
[51] D. Carriazo, M.C. Serrano, M.C. Gutiérrez, et al., Chem. Soc. Rev. 41 (2012) 4996–5014.